J. Plasma Phys. (2023), *vol*. 89, 905890519
Published by Cambridge University Press

doi:10.1017/S0022377823001149

The effect of pressure anisotropy on 3-D MHD stability for low magnetic field LHD equilibria

T.E. Moen [1],†, **Y. Suzuki** [2] **and J.H.E. Proll** [1]

[1]Eindhoven University of Technology, P.O. Box 513, 5600 MB Eindhoven, The Netherlands

[2]Graduate School of Advanced Science and Engineering, Hiroshima University, 1-4-1 Kagamiyama, Higashihiroshima 739-8527, Japan

(Received 3 January 2023; revised 5 October 2023; accepted 5 October 2023)

The magnetohydrodynamic stability of plasmas with an anisotropic pressure component is analysed for a low magnetic field configuration of the large helical device. Magnetic equilibria are calculated by the anisotropic Neumann inverse moments equilibrium code, an extension of the three-dimensional variational moments equilibrium code. A modified version of the bi-Maxwellian is used to model the anisotropic particle velocity distribution. Magnetohydrodynamic stability calculations for the $n = 1$ mode family are carried out by TERPSICHORE, which has been expanded by the Kruskal–Oberman energy principle. For on-axis particle deposition, the growth rate and plasma displacement show that the parallel dominant plasmas are significantly more stable than isotropic or perpendicular dominant plasmas. For off-axis particle deposition, the growth rate and the Mercier criterion in the peripheral region $\rho = 0.9$, show that low field (LF) deposition perpendicular dominant plasmas are most unstable. For the most realistic off-axis deposition profile, it is found that parallel dominant plasmas are most stable for LF deposition, while perpendicular dominant plasmas are most stable for high field deposition. We conclude that, under low magnetic field conditions in the large helical device, tangential neutral beam injection heating has a stabilising influence on the plasma.

Key words: plasma instabilities, plasma simulation, plasma heating

1. Introduction

The Large Helical Device (LHD), a heliotron type stellarator, has achieved a volume-averaged normalised pressure, or beta value, $\langle\beta\rangle$, of over 4 % at low magnetic field (Watanabe *et al.* 2005). Linear ideal magnetohydrodynamics (MHD) stability calculations have been carried out for this operational regime. These have found that MHD instabilities in the peripheral region do not cause drastic degradation of the plasma confinement (Watanabe *et al.* 2005). This is in stark contrast to tokamaks, where operational $\langle\beta\rangle$ limits predicted by the linear ideal MHD theory can often be successfully confirmed by experiment (ITER Physics Basis Editors *et al.* 1999).

† Email address for correspondence: t.e.moen@student.tue.nl

In order to sustain the high-beta plasma in the LHD, heating schemes including neutral beam injection (NBI), ion cyclotron resonance heating (ICRH) and electron cyclotron resonance heating (ECRH) are employed (Motojima *et al.* 2003). These heating schemes sometimes produce a plasma with a non-Maxwellian velocity space distribution depending on the thermal equilibration, which then leads to a pressure anisotropic plasma. In the LHD, the ratio of parallel to perpendicular kinetic energy has been shown to exceed a value of 4 as a consequence of heating through NBI (Yamaguchi *et al.* 2005). Under low magnetic field conditions, the operational $\langle\beta\rangle$ regime of LHD has been shown to cross the theoretical threshold predicted by isotropic, linear MHD theory (Watanabe *et al.* 2005). Although MHD stability analyses have been carried out for LHD plasmas with an anisotropic pressure distribution (Cooper *et al.* 2006*b*, 2007, 2012), the effect of anisotropic plasmas on the operational $\langle\beta\rangle$ regime has not been researched in detail.

The three-dimensional (3-D) equilibrium solver VMEC (variational moments equilibrium code) (Hirshman & Betancourt 1991) has been expanded by separating the parallel and perpendicular components of the plasma pressure to a code called ANIMEC (anisotropic Neumann inverse moments equilibrium code) (Cooper *et al.* 2009). The hot plasma particles are described in this code using either a variant of a bi-Maxwellian distribution (Cooper *et al.* 2006*a*) or a slowing-down distribution (Cooper *et al.* 2005). The 3-D equilibria constructed by ANIMEC can be used to perform ideal linear MHD stability calculations using the TERPSICHORE code (Anderson *et al.* 1990). This code has been expanded to include two energy principles that extend beyond ideal MHD theory, which allows plasmas with a pressure anisotropy to be analysed. The Kruskal–Oberman (KO) principle models the hot-particle species as a fully interacting liquid, enabling it to contribute to pressure- and current-driven instabilities (Kruskal & Oberman 1958). The Johnson–Kulsrud–Weimer model, on the other hand, also known in the literature as the non-interacting (NI) model, simulates the hot-particle species as a non-interacting layer (Johnson, Kulsrud & Weimer 1969).

Building on the analysis of 3-D equilibria of pressure anisotropy in LHD carried out by Romba, Suzuki & Proll (2021), in this work, we analyse the effect of pressure anisotropy on linear 3-D MHD stability using both ANIMEC and TERPSICHORE. In particular, we provide both a qualitative and a quantitative analysis of pressure anisotropy on linear MHD stability for different hot-particle pressure profiles. We consider both on-axis and off-axis particle deposition profiles. For the off-axis profiles, both high field (HF) and low field (LF) deposition simulations are carried out and compared. The MHD stability corresponding to pressure anisotropic plasmas is analysed by investigating the plasma displacement, growth rate and Mercier criterion of global (low-n) MHD modes. This analysis is then used to investigate the effect of pressure anisotropy on plasma stability and the operational $\langle\beta\rangle$ regime of LHD.

Section 2 treats the theory associated with magnetic equilibria in the context of pressure anisotropy. Section 3 introduces the theory behind linear MHD stability for pressure anisotropic plasmas and discusses two energy principles that extend isotropic MHD theory. Section 4 describes the magnetic equilibrium of the plasmas that will be simulated. Next, in § 5, the result of the MHD stability calculations pertaining to the equilibria described in the previous section is analysed. Finally, § 6 summarises the results and looks at possible future research that could extend this work.

2. Numerical equilibrium theory

Magnetohydrodynamic equilibrium codes employ energy minimisation techniques to calculate a plasma equilibrium. The total energy minimised in VMEC and ANIMEC comprises a potential and kinetic energy part. The former is associated with magnetic

https://doi.org/10.1017/S0022377823001149 Published online by Cambridge University Press

pressure and the latter with plasma pressure. The total energy functional used in ANIMEC is given by (Cooper *et al.* 1992),

$$W = \int \mathrm{d}^3x \left(\frac{B^2}{2\mu_0} + \frac{p_\parallel(s,B)}{\Gamma - 1} \right), \tag{2.1}$$

where B denotes the local magnetic field strength, μ_0 is the permeability of free space ($4\pi \times 10^{-7}\,\mathrm{H\,m^{-1}}$) and Γ is the adiabatic index, which is usually set to zero. The total parallel particle pressure $p_\parallel(s,B)$, is a function of the flux surface coordinate $s \in [0,1]$, which is proportional to the toroidal magnetic flux $2\pi\Phi$ enclosed, and of the magnetic field strength B. Note that the normalised radial coordinate ρ relates to the flux surface coordinate s as $s = \rho^2$. It has been shown that (2.1) can be manipulated such that the ideal MHD equilibrium force is recovered (Cooper *et al.* 1992)

$$\boldsymbol{F} = -\nabla \cdot \boldsymbol{P} + \boldsymbol{j} \times \boldsymbol{B}. \tag{2.2}$$

In this equation, $\boldsymbol{P}$ is the pressure tensor given by (Chew *et al.* 1956)

$$\boldsymbol{P} = p_\perp \boldsymbol{I} + (p_\parallel - p_\perp)\boldsymbol{bb}, \tag{2.3}$$

where $p_\perp$ and $p_\parallel$ are the total perpendicular and parallel pressures, respectively, $\boldsymbol{I}$ is the unit matrix, $\boldsymbol{b} = \boldsymbol{B}/B$ is the unit vector in the direction of the magnetic field lines and $\boldsymbol{j}$ is the current density. Given that the parallel pressure is a function of B, this quantity, and by extension the perpendicular pressure, are not flux surface quantities, as opposed to the total pressure. The parallel pressure comprises a part due to thermal particles and a part due to hot particles. With the adiabatic index set to zero, the total parallel pressure takes the form (Cooper *et al.* 1992)

$$p_\parallel(s,B) = M(s)\left[1 + p_h(s)H(s,B)\right], \tag{2.4}$$

where $M(s)$ is the plasma mass, $p_h(s)$ is the hot-particle pressure component and $H(s,B)$ is a factor that describes the change in total parallel pressure around a magnetic flux surface. The hot-particle term in this equation introduces an anisotropy through the dependence of H on the magnetic field. For completeness, the force balance describing the calculation of the total perpendicular pressure is given by

$$p_\perp(s,B) = p_\parallel(s,B) - B\left.\frac{\partial p_\parallel}{\partial B}\right|_s. \tag{2.5}$$

The hot particles modelled by ANIMEC are described by a variant of the bi-Maxwellian distribution (Cooper *et al.* 2006*a*)

$$\mathcal{F}_h(s,\mathcal{E},\mu) = \mathcal{N}(s)\left(\frac{m_h}{2\pi T_\perp(s)}\right)^{3/2} \exp\left[-m_h\left(\frac{\mu B_C}{T_\perp(s)} + \frac{|\mathcal{E} - \mu B_C|}{T_\parallel(s)}\right)\right]. \tag{2.6}$$

In this equation $\mathcal{E}$ and μ represent the total particle energy and the particle magnetic moment, respectively. These parameters can be rewritten to obtain an equivalent description in terms of $v_\parallel$ and $v_\perp$, the parallel and perpendicular particle velocity components. The parameters $\mathcal{N}(s)$, m_h, $T_\perp(s)$ and $T_\parallel(s)$ describe a density-like amplitude, the hot-particle mass and the perpendicular and parallel components of the plasma temperature, respectively. The parameter B_C, called the critical magnetic field, determines the number of trapped particles in the fusion device. This is a consequence of the fact that most hot particles are deposited near the location where $B = B_C$. This variant of the bi-Maxwellian distribution has been shown to satisfy the lowest-order solution to the Fokker–Planck equation $\boldsymbol{B} \cdot \nabla \mathcal{F}_h = 0$ (Dendy *et al.* 1995).

https://doi.org/10.1017/S0022377823001149 Published online by Cambridge University Press

3. Linear MHD stability theory

Two energy principles have been implemented in the TERPSICHORE code: the fully interacting KO principle (Kruskal & Oberman 1958) and the non-interacting NI model (Johnson *et al.* 1969). These energy principles fundamentally differ in the way they treat hot-particle species in the context of pressure- and current-driven instabilities. The KO model incorporates the effect of hot particles on MHD instabilities, while the NI model describes hot particles as non-interacting, therefore affecting MHD instabilities only indirectly. In this research we focus on the KO energy principle, given that this model forms the most comprehensive framework for studying the effect that different hot-particle pressure profiles have on pressure- and current-driven instabilities.

The TERPSICHORE code solves the following eigenvalue equation:

$$\langle \delta W_P \rangle + \langle \delta W_V \rangle - \omega^2 \langle \delta W_K \rangle = 0, \tag{3.1}$$

where δW_P, δW_V and δW_K denote the plasma potential energy, the vacuum energy and the kinetic energy. The variable $\langle W \rangle$ denotes the volume average of the energy W. The plasma potential energy can be subdivided into the following components:

$$\langle \delta W_P \rangle = \langle \delta W_{C^2} \rangle + \langle \delta W_{\mathrm{BI}} \rangle + \langle \delta W_J \rangle, \tag{3.2}$$

where W_{C^2} represents a positive definite stabilising component, which is associated with magnetic field line bending and compression as well as plasma compression; W_{BI} represents pressure driven instabilities such as ballooning and interchange modes and W_J represents parallel current driven kink modes. In TERPSICHORE, the terms in (3.2) are evaluated in Boozer coordinates, which allows the eigenvalue problem to be separated into individual Fourier components (Boozer 1980).

In ideal MHD theory with isotropic pressure, the term in (3.2) that describes pressure-driven instabilities is given by

$$\langle \delta W_{\mathrm{BI}} \rangle = -\int \mathrm{d}^3 x (\boldsymbol{\xi}_\perp \cdot \nabla p)(\boldsymbol{\xi}_\perp^* \cdot \boldsymbol{\kappa}), \tag{3.3}$$

where $\boldsymbol{\xi}$ denotes the plasma displacement vector, p the pressure and $\boldsymbol{\kappa}$ the curvature vector of the magnetic flux surface. The asterisk denotes complex conjugation. By modelling the plasma as an incompressible fluid, the plasma displacement can be written as follows (Anderson *et al.* 1990):

$$\boldsymbol{\xi} = \sqrt{g}\xi^s \nabla\theta \times \nabla\phi + \eta \frac{\boldsymbol{B} \times \nabla s}{B^2}, \tag{3.4}$$

where ξ^s and η are the radial and binormal components of $\boldsymbol{\xi}$, respectively, and $\sqrt{g}$ is the Jacobian describing the transformation from Cartesian to Boozer coordinates. Due to the incompressibility constraint, the component of $\boldsymbol{\xi}$ parallel to the field lines vanishes.

The KO and NI energy principles expand on the equation above by introducing pressure anisotropy. When expressing the corresponding energy term in the KO energy principle in Boozer coordinates (Boozer 1980), the following expression is obtained (Grad 1966;

https://doi.org/10.1017/S0022377823001149 Published online by Cambridge University Press

Cooper *et al.* 2006*b*):

$$\delta W_{\mathrm{BI}}(s) = -\frac{1}{2}\int_0^{2\pi/L_s} \mathrm{d}\phi \int_0^{2\pi} \mathrm{d}\theta \left(\frac{\tau}{\tau+\sigma}\right)\left(\frac{1}{\sigma B^2}\right)\left(\left.\frac{\partial p_\parallel}{\partial s}\right|_B + \frac{\sigma}{\tau}\left.\frac{\partial p_\perp}{\partial s}\right|_B\right)(\xi^s)^2$$
$$\times\left[\sqrt{g}\left(\left.\frac{\partial p_\parallel}{\partial s}\right|_B + \frac{\sigma}{\tau}\left.\frac{\partial p_\perp}{\partial s}\right|_B\right) + \psi''(s)J(s) - \Phi''(s)I(s)\right.$$
$$\left. + \psi'(s)J'(s) - \Phi'(s)I'(s) + \sigma B_s(\boldsymbol{B}\cdot\nabla\sqrt{g}) - \sigma B^2\frac{\partial\sqrt{g}}{\partial s}\right]. \tag{3.5}$$

In this equation τ and σ refer to the mirror and firehose stability criteria, $2\pi\Psi$, $2\pi I$ and $2\pi J$ refer, respectively, to the poloidal magnetic flux, the effective poloidal current flux and effective toroidal current flux and L_s refers to the number of field periods within one toroidal period. This equation shows that the hot-particle pressures, which are contained in the terms $p_\parallel$ and $p_\perp$, have a direct influence on the energy balance.

The TERPSICHORE code is a linear MHD code which returns an eigenvalue corresponding to the growth rate of the most dominant linear MHD instability as well as the corresponding eigenvector which describes the plasma displacement. The TERPSICHORE code has, however, been expanded to return quasi-linear parameters such as physical values for the kinetic energy and a calculation of the Mercier criterion for both the KO and NI energy principles (Cooper 1992). Growth rates, plasma displacements and Mercier criteria are analysed in § 5.

4. Equilibrium calculations

The 3-D magnetic equilibria required to perform MHD stability analysis have been simulated using ANIMEC with fixed boundary conditions. In this work, the last closed magnetic flux surface has been chosen to represent the LHD standard configuration. The pressure anisotropy can be input in ANIMEC by specifying $T_\perp/T_\parallel$ as a function of s. In this work we have set the ratio $T_\perp/T_\parallel$ to a constant value. In order to better capture the degree of pressure anisotropy in the plasma, the following parameter will be used to characterise magnetic equilibria:

$$\langle\beta_{\perp/\parallel}\rangle \equiv \frac{\langle\beta_\perp\rangle}{\langle\beta_\parallel\rangle}. \tag{4.1}$$

The following definitions are employed:

$$\langle\beta\rangle = \frac{\frac{1}{3}\int \mathrm{d}^3x(p_\parallel + 2p_\perp)}{\int \mathrm{d}^3x\frac{B^2}{2\mu_0}}, \tag{4.2a}$$

$$\langle\beta_\perp\rangle = \frac{\int \mathrm{d}^3x p_\perp}{\int \mathrm{d}^3x\frac{B^2}{2\mu_0}}, \tag{4.2b}$$

$$\langle\beta_\parallel\rangle = \frac{\int \mathrm{d}^3x p_\parallel}{\int \mathrm{d}^3x\frac{B^2}{2\mu_0}}. \tag{4.2c}$$

https://doi.org/10.1017/S0022377823001149 Published online by Cambridge University Press

Name	$p_h \propto$	B_C values (T)	Heating scheme
Parabolic	$1 - s$	2.7	NBI
Peaked	$(1 - s)^2$	2.7	ECRH, ICRH
Broad	$1 - s^2$	2.7	NBI
Hollow	$s(1 - s)$	2.3, 3.1	ECRH, ICRH, NBI
Realistic	$1 - s^2 + s(1 - s)$	2.3, 3.1	NBI

TABLE 1. The hot-particle pressure profiles for which MHD stability analysis has been performed, along with the values for B_C chosen for simulation and the corresponding heating scheme.

We approximate the fraction $\langle\beta_h\rangle/\langle\beta\rangle \approx 1/3$ for all simulations in this work, unless otherwise specified. For all simulations $\langle\beta\rangle$ is scanned over the set $\langle\beta\rangle \in \{0.5\,\%, 1.0\,\%, \ldots, 3.5\,\%\}$. The perpendicular to parallel pressure ratio was approximated to be $\langle\beta_{\perp/\parallel}\rangle \in \{1/4, 1, 4\}$, corresponding to parallel dominant, isotropic and perpendicular dominant plasmas, respectively. It should be noted that this pressure ratio strongly depends on the thermal- and hot-pressure profiles. The thermal-pressure profile has been set to a parabolic profile $p_{\text{th}} \propto 1 - s$, which approximates experimental observations (Watanabe *et al.* 2005). The hot-particle pressure profiles used in this work are described in table 1. These hot-particle pressure profiles have been chosen to be able to simulate the effect of pressure anisotropy in the context of different heating schemes. The table lists the B_C values for which simulations have been carried out and the heating methods that most accurately describe the corresponding hot-pressure profile. The values $B_C = 2.3\,\text{T}, 3.1\,\text{T}$ correspond to LF and HF deposition. Note that, for pressure isotropic simulations, a value of $B_C = 1.0\text{T}$ has been used. For isotropic simulations, $T_\parallel(s) = T_\perp(s)$, which, in combination with the value of $B_C = 1.0\text{T}$, reduces the bi-Maxwellian given in (2.6) to a Maxwellian distribution. Figure 1 displays the hot-pressure profiles as a function of the flux surface coordinate s. The parabolic, peaked and broad profiles have a maximum at $s = 0$, corresponding to on-axis hot-particle deposition, whereas the hollow and realistic profiles correspond to off-axis deposition.

The magnetic equilibrium computed by ANIMEC can be analysed by investigating the parallel and perpendicular components of the hot-particle pressure distribution. For the example case of the perpendicular dominant realistic hot-particle profile, figures 2 and 3 show the parallel and perpendicular components of the hot-particle distribution, respectively, overlapped by flux surfaces. From these plots, it is observed that neither component of the hot-particle distribution is a flux surface quantity. The perpendicular hot-particle pressure shows two clear local maxima. This can be explained by the fact that the perpendicular component of the ion velocity is highest near the reflection points of trapped particles. The shape of the perpendicular hot-particle pressure distribution implies the existence of high pressure gradients which can negatively impact plasma stability. Also, these gradients impose a threshold on the maximum $\langle\beta\rangle$ value that can be simulated. Both the hot- and thermal-pressure distributions have an effect on the local effective magnetic field, which in turn affects the rotational transform profile, $\iota(s)$. The rotational transform profile of two example cases and a vacuum simulation are shown in figure 4. The rotational transform of the LHD is negative everywhere inside the fusion device. In this work, however, the rotational transform will be presented as a positive value for readability

https://doi.org/10.1017/S0022377823001149 Published online by Cambridge University Press

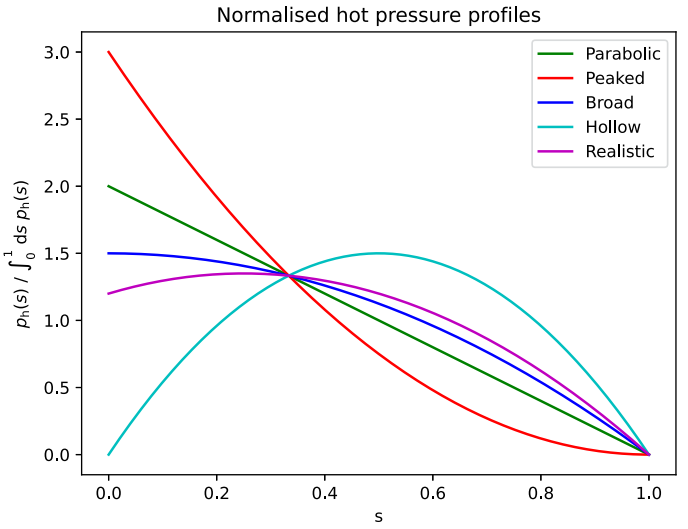

FIGURE 1. The normalised hot-particle pressure profiles p_h described in table 1, as a function of the flux surface coordinate s.

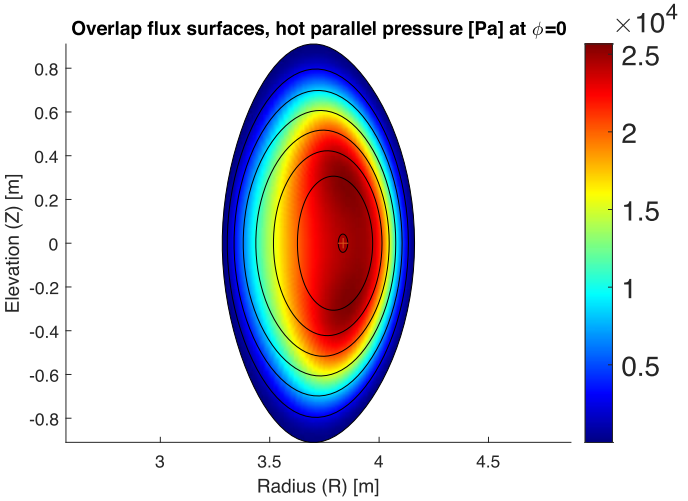

FIGURE 2. Hot-particle parallel pressure distribution for the realistic hot-pressure profile with $B_C = 2.3$T and $\langle\beta\rangle \approx 3\,\%$ in a vertically elongated cross-section. The black curves indicate flux surfaces.

of the figures. Note that, under specific conditions, the magnetic shear can vanish close to the magnetic axis.

5. The MHD stability results

The MHD stability code TERPSICHORE will be used to analyse the $n = 1$ mode family of instabilities (Cooper *et al.* 1990; Nührenberg née Schwab 1993; Ardelea & Cooper 1997). The $n = 1$ mode family is analysed, because experiment shows that the most dominant MHD instabilities in LHD belong to this particular mode family (Watanabe *et al.* 2005). The growth rate, plasma displacement vector $\boldsymbol{\xi}$ and Mercier criterion corresponding

https://doi.org/10.1017/S0022377823001149 Published online by Cambridge University Press

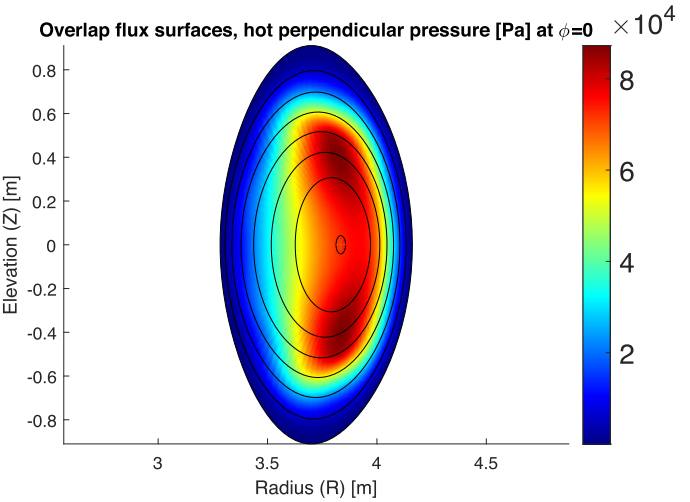

FIGURE 3. Hot-particle perpendicular pressure distribution for the realistic hot-pressure profile with $B_C = 2.3\text{T}$ and $\langle\beta\rangle \approx 3\,\%$ in a vertically elongated cross-section. The black curves indicate flux surfaces.

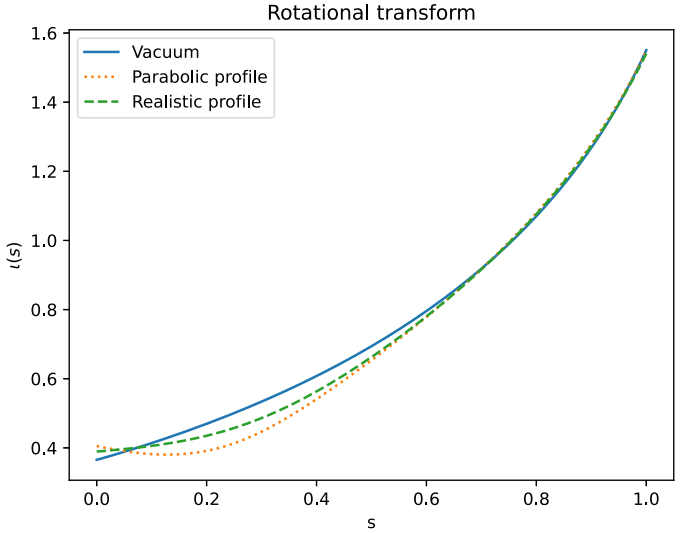

FIGURE 4. Rotational transform $\iota(s)$ for a vacuum simulation and for the parabolic and realistic hot-pressure profiles at pressure isotropy. For the latter two profiles, $\langle\beta\rangle \approx 2.5\,\%$ and $\langle\beta\rangle \approx 3\,\%$, respectively.

to the KO energy principle (Cooper *et al.* 2006*b*) will be analysed in this section. The plasma displacement vector $\boldsymbol{\xi}$ will be analysed through its modal structure as a function of the flux surface coordinate s. For every hot-particle pressure profile, the maximum $\langle\beta\rangle$ simulation that would converge in both ANIMEC and TERPSICHORE is treated. This implies that, especially for on-axis heating profiles, the $\langle\beta\rangle$ value shown can be significantly lower than the maximum of the $\langle\beta\rangle$ scan.

https://doi.org/10.1017/S0022377823001149 Published online by Cambridge University Press

The plasma displacement sum over all modes will be used to compare the plasma displacement between different levels of anisotropy

$$\Xi(s) = \sum_{k=1}^{K} \xi_{n_k,m_k}(s), \tag{5.1}$$

where K is the total number of computed modes, $\{n_k\}$ and $\{m_k\}$ are sequences containing toroidal and poloidal mode numbers, respectively, sorted based on maximum amplitude and where

$$\boldsymbol{\xi}_{n,m}(s) = \xi_{n,m}(s) \cdot \hat{\boldsymbol{\xi}}_{n,m}(s). \tag{5.2}$$

Note that the unit vector $\hat{\boldsymbol{\xi}}_{n,m}(s)$ is normal to the flux surface s and is pointing away from the magnetic axis. The sequences $\{n_k\}$ and $\{m_k\}$ are constructed such that

$$\max_{s\in[0,1]} |\xi_{n_1,m_1}(s)| \geq \max_{s\in[0,1]} |\xi_{n_2,m_2}(s)| \geq \cdots \geq \max_{s\in[0,1]} |\xi_{n_K,m_K}(s)|. \tag{5.3}$$

Note also that the eigenvector $\boldsymbol{\xi}$ calculated by TERPSICHORE can be scaled arbitrarily. The figures containing $\Xi(s)$ throughout this work illustrate the direct results from calculations performed by TERPSICHORE and have not been rescaled.

5.1. *On-axis deposition profiles*

Figure 5 shows the graph of $\Xi(s)$ for the parabolic, peaked and broad hot-particle pressure profiles, normalised per simulation result by the maximum value $\Xi_{\max} \equiv \max_{s\in[0,1]} \Xi(s)$. The mode width of the plasma displacement is observed to be significantly smaller for parallel dominant plasmas for all on-axis deposition profiles, while the differences between the isotropic and perpendicular dominant cases are negligible. In global mode analysis, this mode width directly relates to the growth rate (Sugama & Wakatani 1989; Gupta, Callen & Hegna 2002). Moreover, the mode width pertaining to the plasma displacement is proportional to the volume of plasma displaced. Thus, following from (3.5), this difference in mode width indicates that the energy associated with the plasma displacement is smallest for parallel dominant plasmas for on-axis profiles, which is conducive to plasma stability. A shift in $s_{\max}$, the flux surface coordinate s for which the plasma displacement is largest, is also observed with $s_{\max}$ decreasing for increasing $\langle\beta_{\perp/\parallel}\rangle$. The change in $s_{\max}$ is a direct consequence of the change in shape of the $\iota(s)$ profile for different hot-pressure profiles. The underlying mode structure of the displacement vector is shown in figure 6 for an example case that corresponds to a pressure isotropic simulation of the parabolic hot-particle pressure profile. This figure also shows the graph of the rotational transform $\iota(s)$, which allows us to conclude that the most dominant mode is the resonant $n = 1, m = 2$ mode at the $\iota = 0.5$ surface. The mode structure for the parabolic, peaked and broad hot-particle profiles look very similar.

The growth rates corresponding to the eigenvalues found in (3.1) are shown in figure 7. From the growth rates we conclude that the plasma becomes more unstable for increasing $\langle\beta_{\perp/\parallel}\rangle$ for all on-axis deposition profiles. Noticeably, for high $\langle\beta\rangle$ values, parallel dominant plasmas have significantly lower growth rates than isotropic or perpendicular dominant plasmas, which is in agreement with the plasma displacement results. Analysing the mode structure of the plasma displacement for the on-axis deposition profiles, it is concluded that the $n = 1, m = 2$ is present and dominant for all $\langle\beta\rangle$ values. The Mercier criteria at $s = 0.81$ ($\rho = 0.9$) corresponding to the on-axis deposition profiles are shown in figure 8.

https://doi.org/10.1017/S0022377823001149 Published online by Cambridge University Press

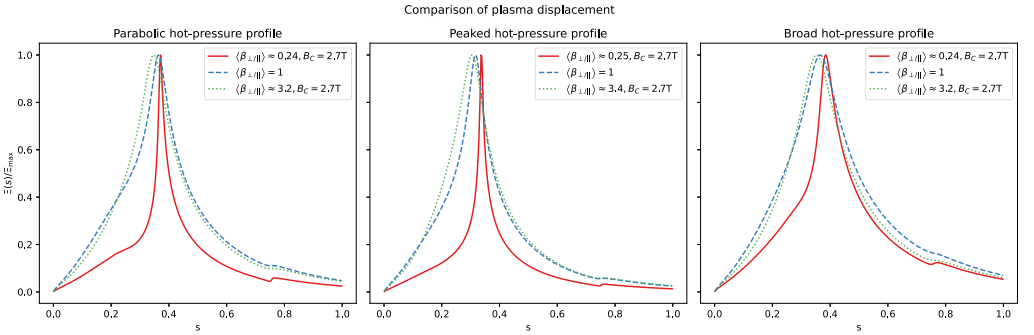

FIGURE 5. The normalised plasma displacement sum over all modes as a function of the flux surface coordinate s, $\Xi(s)/\Xi_{\max}$, for the parabolic, peaked and broad hot-particle pressure profiles. For each profile, three levels of anisotropy were considered. The $\langle\beta\rangle$ values for the parabolic, peaked and broad profiles are approximately equal to 2.5 %, 1.5 % and 3 %, respectively.

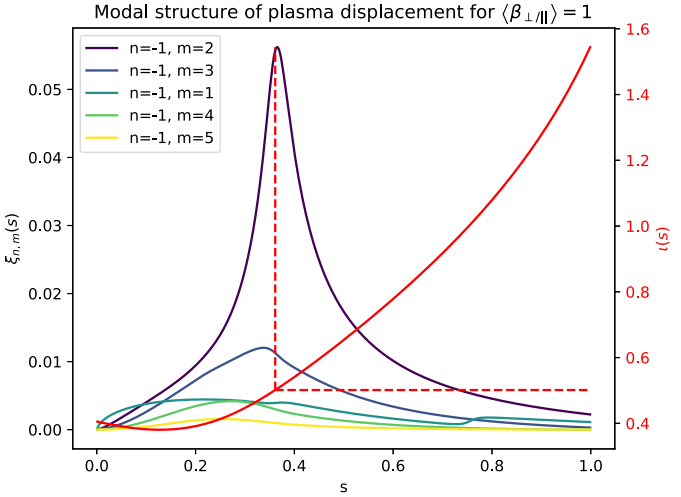

FIGURE 6. The five most dominant modes in line with ordering in (5.3) of the displacement vector and the ι profile for a parabolic hot-pressure profile. This figure shows a pressure isotropic simulation with $\langle\beta\rangle \approx 2.5$ %. The red dotted lines indicate the location of the $\iota(s) = 0.5$ surface.

5.2. *Off-axis deposition profiles*

The hollow and realistic hot-particle pressure profile simulations contain an additional parameter B_C, which has been scanned over to vary the deposition location of the hot-particle species. Figure 9 shows $\Xi(s)$ corresponding to the hollow and realistic off-axis deposition profiles for varying pressure anisotropy and critical magnetic field B_C. It is found that, for parallel dominant plasmas, the value of B_C has a negligible effect on the plasma displacement $\Xi(s)$. This can be explained by the fact that the trapped particle fraction for parallel dominant plasmas is relatively low compared with perpendicular dominant plasmas. From this figure, we can also conclude that LF deposition of perpendicular dominant ions has a pronounced destabilising effect for both hot-pressure profiles. This is corroborated by figure 10, which shows the growth rates corresponding

https://doi.org/10.1017/S0022377823001149 Published online by Cambridge University Press

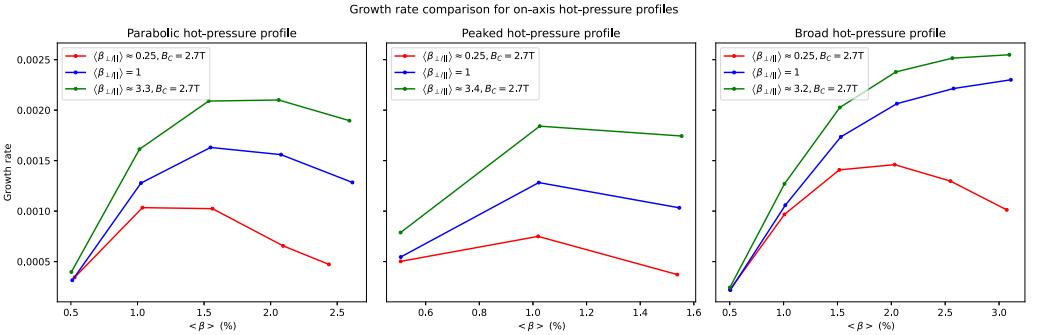

FIGURE 7. The growth rates corresponding to the parabolic, peaked and broad hot-particle pressure profiles. For each profile, three levels of anisotropy were considered. The $\langle\beta\rangle$ values for the parabolic, peaked and broad profiles are approximately equal to 2.5 %, 1.5 % and 3 %, respectively. The value for $\langle\beta_{\perp/\parallel}\rangle$ represents the average value over all simulations in the $\langle\beta\rangle$-scan with the same ratio $T_\perp/T_\parallel$.

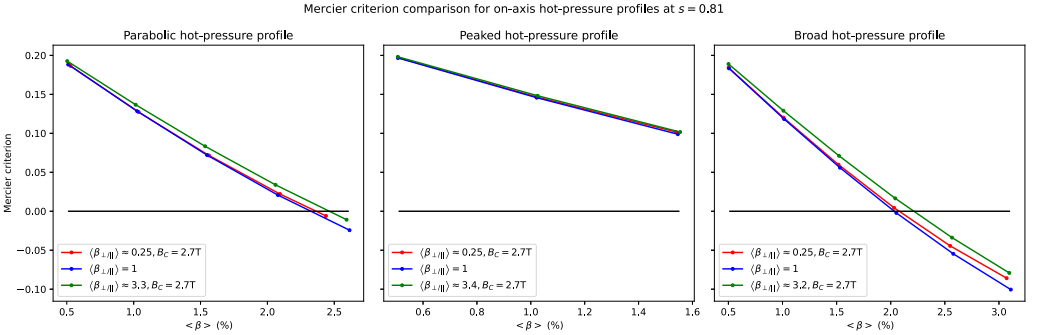

FIGURE 8. The Mercier criteria corresponding to the parabolic, peaked and broad hot-particle pressure profiles. For each profile, three levels of anisotropy were considered. The $\langle\beta\rangle$ values for the parabolic, peaked and broad profiles are approximately equal to 2.5 %, 1.5 % and 3 %, respectively. The value for $\langle\beta_{\perp/\parallel}\rangle$ represents the average value over all simulations in the $\langle\beta\rangle$-scan with the same ratio $T_\perp/T_\parallel$. The black lines indicate the stability boundary where the Mercier criterion is zero.

to the simulations of the off-axis deposition profiles. The growth rates pertaining to the perpendicular dominant plasmas for both hot-pressure profiles are observed to decrease substantially when transitioning from LF to HF deposition. The realistic profile shows the only case in all simulations carried out for which a perpendicular dominant plasma in the context of the same hot-pressure profile appears to be more stable than parallel dominant plasmas. It is observed in figure 10 that the growth rate is more sensitive to the plasma anisotropy ratio $\langle\beta_{\perp/\parallel}\rangle$ for LF deposition than for HF deposition for both the hollow and realistic hot-particle pressure profiles. This result is in agreement with the eigenvalue analysis performed for the mode family $n = 2$ for the hollow profile in Cooper *et al.* (2007).

In the case of a hollow hot-pressure profile, the $n = 1, m = 1$ mode component is clearly visible, peaking at $s \approx 0.75$, and is most pronounced for the parallel dominant case. The Mercier criteria at $s = 0.81$ corresponding to the off-axis deposition profiles are shown in figure 11. As opposed to the Mercier criteria for on-axis profiles, figure 8, a large change

https://doi.org/10.1017/S0022377823001149 Published online by Cambridge University Press

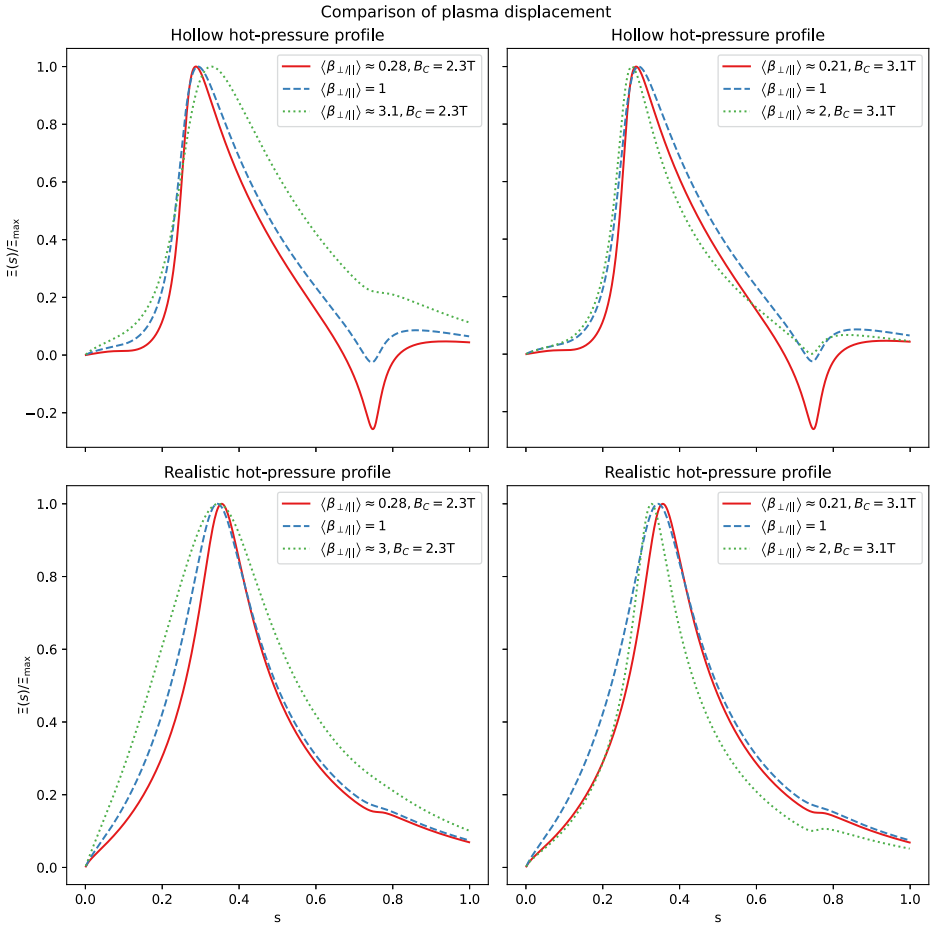

FIGURE 9. The function $\Xi(s)/\Xi_{\max}$ for the hollow and realistic hot-particle pressure profiles. For each profile, three levels of anisotropy were considered. For both pressure profiles, $\langle\beta\rangle \approx 3\,\%$.

in Mercier criterion value is observed in the case of perpendicular dominant plasmas. For perpendicular dominant plasmas, the Mercier criterion value crosses the stability boundary at a lower value of $\langle\beta\rangle$. The results shown in figure 11 are in agreement with the results corresponding to the plasma displacement and growth rate to some degree. The main discrepancy that exists for both hot-pressure profiles is the fact that the difference in Mercier criteria for the isotropic and parallel dominant cases is negligible, while the difference in growth rate is substantial, for high values of $\langle\beta\rangle$.

6. Conclusion

The 3-D magnetic equilibrium and linear MHD stability have been calculated for anisotropic plasmas in the case of the LHD stellarator for a low magnetic field configuration and have been compared with isotropic plasmas. The magnetic equilibrium has been calculated using the ANIMEC code, while TERPSICHORE has been used for the linear MHD stability calculations. A modified version of the bi-Maxwellian was used to model the effect of pressure anisotropy on the particle velocity distribution. In the simulations carried out, we chose a parabolic thermal-pressure profile in order to match

https://doi.org/10.1017/S0022377823001149 Published online by Cambridge University Press

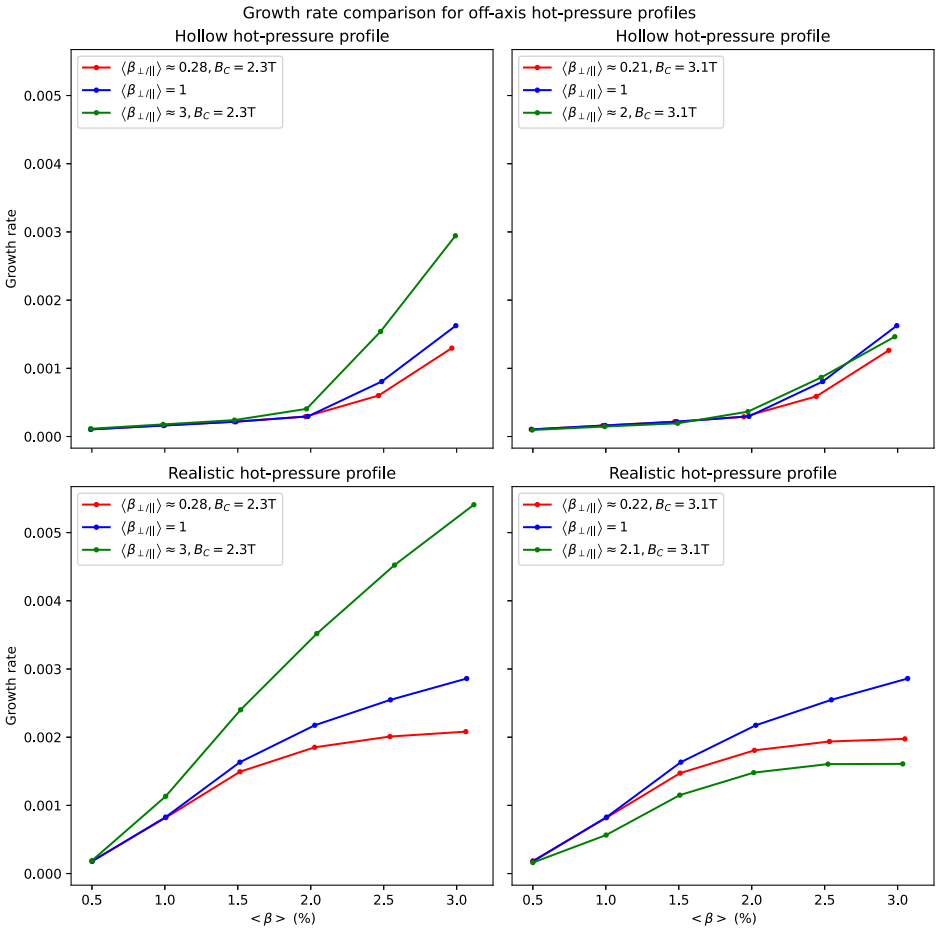

FIGURE 10. The growth rates corresponding to the hollow and realistic hot-particle pressure profiles. For each profile, three levels of anisotropy were considered. For both pressure profiles, $\langle\beta\rangle \approx 3\,\%$. The value for $\langle\beta_{\perp/\|}\rangle$ represents the average value over all simulations in the $\langle\beta\rangle$-scan with the same ratio $T_\perp/T_\|$.

experimental conditions. Five hot-particle pressure profiles were analysed, three of which correspond with on-axis particle deposition and two with off-axis deposition. The KO energy principle, which has been implemented in TERPSICHORE, has been used to calculate the following stability parameters: the growth rate, the mode structure of the plasma displacement and the Mercier criterion at $s = 0.81$. The $n = 1$ mode family has been analysed in TERPSICHORE.

The growth rates for the on-axis hot-particle pressure profiles reveal a clear dependence on the level of anisotropy $\langle\beta_{\perp/\|}\rangle$. For all $\langle\beta\rangle > 0.5\,\%$, the growth rate is observed to increase for increasing $\langle\beta_{\perp/\|}\rangle$, regardless of the specific profile shape. The plasma displacement for parallel dominant plasmas is observed to have a small mode width in comparison with the isotropic and perpendicular cases. These two facts combined allows us to conclude that the parallel dominant case represents the most stable plasma configuration and is noticeably more stable than the more common case of plasma isotropy. For the off-axis hot-particle pressure profiles, the plasma displacement, growth rate and Mercier criterion at $s = 0.81$ show that perpendicular dominant plasmas with LF

https://doi.org/10.1017/S0022377823001149 Published online by Cambridge University Press

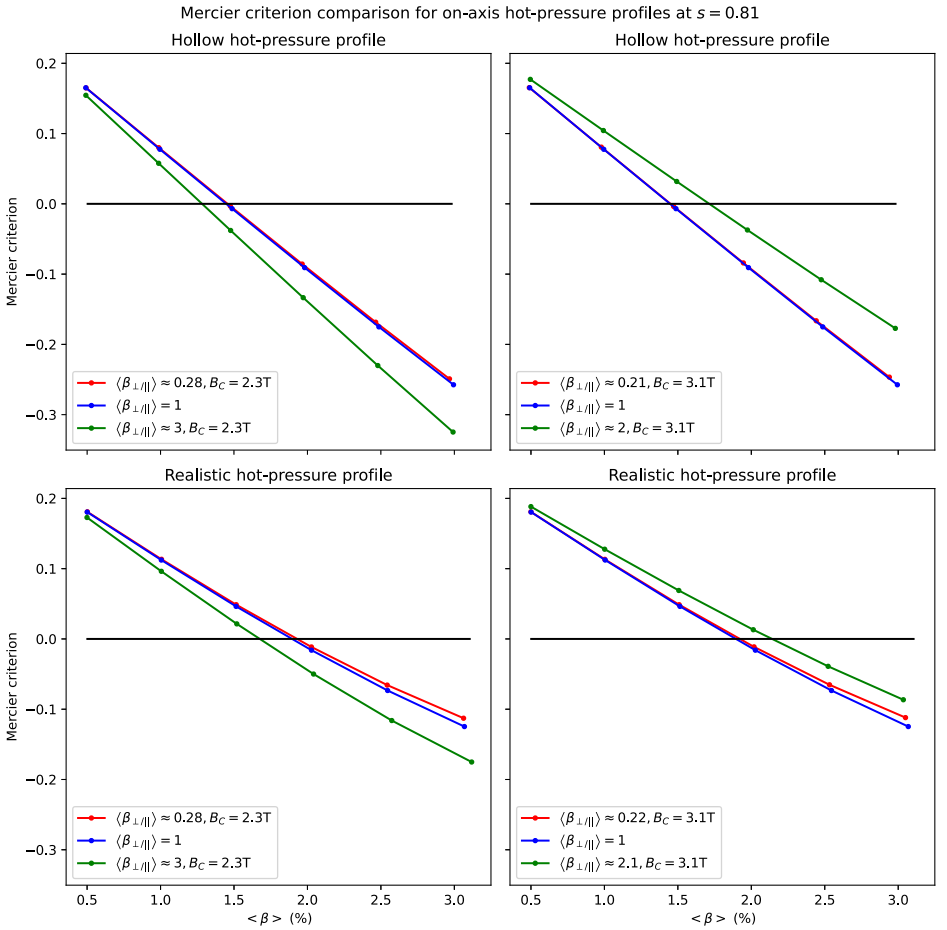

FIGURE 11. The Mercier criteria corresponding to the hollow and realistic hot-particle pressure profiles. For each profile, three levels of anisotropy were considered. For both pressure profiles, $\langle\beta\rangle \approx 3\,\%$. The value for $\langle\beta_{\perp/\parallel}\rangle$ represents the average value over all simulations in the $\langle\beta\rangle$-scan with the same ratio $T_\perp/T_\parallel$. The black lines indicate the stability boundary where the Mercier criterion is zero.

deposition are very unstable compared with all other plasma configurations. The Mercier criterion shows a clear discrepancy in stability between perpendicular dominant plasmas on the one hand and isotropic and parallel dominant plasmas on the other. For the realistic hot-pressure profile, perpendicular dominant plasmas with HF deposition are found to be most stable. For LF deposition, however, parallel dominant plasmas are found to be most stable for this profile. We can conclude that the fact that the theoretical threshold for isotropic plasmas is found to be crossed under a low magnetic field configuration for LHD can be attributed to anisotropy in plasmas. Specifically, tangential NBI heating, which is used as a main heating scheme in LHD, is found to stabilise such plasmas.

Future research could concentrate on the treatment of higher-order modes such as the $n = 2$ mode in TERPSICHORE. This could form a more comprehensive picture of the effect of pressure anisotropy on plasma stability. Another topic for future research is to expand on this work by calculating equilibria using the slowing-down distribution. This distribution is generally found to be more relevant and accurate in modelling NBI heating.

https://doi.org/10.1017/S0022377823001149 Published online by Cambridge University Press

Our work provides a theoretical treatment of the effect of pressure anisotropy on plasma stability. Further research, however, is needed to provide a connection between MHD stability theory and experiment, where experimental research such as that provided by Watanabe *et al.* (2005) should be taken into account.

Acknowledgements

Editor Tünde Fülöp thanks the referees for their advice in evaluating this article.

Funding

This work has been carried out within the framework of the EUROfusion Consortium, funded by the European Union via the Euratom Research and Training Programme (Grant Agreement No 101052200 – EUROfusion). Views and opinions expressed are, however, those of the author(s) only and do not necessarily reflect those of the European Union or the European Commission. Neither the European Union nor the European Commission can be held responsible for them. This work was also partially supported by 'PLADyS', JSPS (Japan Society of the Promotion of Science) Core-to-Core Program, A. Advanced Research Network.

Declaration of interests

The authors report no conflict of interest.

Data availability statement

The data that support the findings of this study are available from the corresponding author, T.E. Moen, upon reasonable request.

REFERENCES

ANDERSON, D.V., COOPER, W.A., GRUBER, R., MERAZZI, S. & SCHWENN, U. 1990 TERPSICHORE: a three-dimensional ideal magnetohydrodynamic stability program. In *Scientific Computing on Supercomputers II* (ed. J.T. Devreese & P.E. Van Camp), pp. 159–174. Springer.

ARDELEA, A. & COOPER, W.A. 1997 External kinks in plasmas with helical boundary deformation and net toroidal current. *Phys. Plasmas* **4** (10), 3482–3492.

BOOZER, A.H. 1980 Guiding center drift equations. *Phys. Fluids* **23** (5), 904–908.

CHEW, G.F., GOLDBERGER, M.L., LOW, F.E. & CHANDRASEKHAR, S. 1956 The Boltzmann equation and the one-fluid hydromagnetic equations in the absence of particle collisions. *Proc. R. Soc. Lond.* A **236** (1204), 112–118.

COOPER, W.A. 1992 Variational formulation of the linear MHD stability of 3D plasmas with noninteracting hot electrons. *Plasma Phys. Control. Fusion* **34** (6), 1011–1036.

COOPER, W.A., ASAHI, Y., NARUSHIMA, Y., SUZUKI, Y., WATANABE, K.Y., GRAVES, J.P. & ISAEV, M.Y. 2012 Equilibrium and stability in a heliotron with anisotropic hot particle slowing-down distribution. *Phys. Plasmas* **19** (10), 102503.

COOPER, W.A., FU, G.Y., GRUBER, R., MERAZZI, S., SCHWENN, U. & ANDERSON, D.V. 1990 In *Proc. Varenna-Lausanne Int. Workshop on Theory of Fusion Plasmas*, p. 655. Editrice Compositori.

COOPER, W.A., GRAVES, J.P., HIRSHMAN, S.P., YAMAGUCHI, T., NARUSHIMA, Y., OKAMURA, S., SAKAKIBARA, S., SUZUKI, C., WATANABE, K.Y., YAMADA, H., *et al.* 2006*a* Anisotropic pressure bi-Maxwellian distribution function model for three-dimensional equilibria. *Nucl. Fusion* **46** (7), 683–698.

COOPER, W.A., GRAVES, J.P., JUCKER, M., WATANABE, K.Y., NARUSHIMA, Y. & YAMAGUCHI, T. 2007 Fluid magnetohydrodynamic stability in a Heliotron with anisotropic fast particle species. *Plasma Phys. Control. Fusion* **49** (8), 1177–1191.

COOPER, W.A., GRAVES, J.P., TRAN, T.M., GRUBER, R., YAMAGUCHI, T., NARUSHIMA, Y., OKAMURA, S., SAKAKIBARA, S., SUZUKI, C., WATANABE, K.Y., *et al.* 2006*b* Stability

properties of anisotropic pressure stellarator plasmas with fluid and noninteractive energetic particles. *Fusion Sci. Technol*. **50** (2), 245–257.

COOPER, W.A., HIRSHMAN, S.P., MERAZZI, S. & GRUBER, R. 1992 3D magnetohydrodynamic equilibria with anisotropic pressure. *Comput. Phys. Commun*. **72** (1), 1–13.

COOPER, W.A., HIRSHMAN, S.P., MERKEL, P., GRAVES, J.P., KISSLINGER, J., WOBIG, H.F.G., NARUSHIMA, Y., OKAMURA, S. & WATANABE, K.Y. 2009 Three-dimensional anisotropic pressure free boundary equilibria. *Comput. Phys. Commun*. **180** (9), 1524–1533.

COOPER, W.A., HIRSHMAN, S.P., YAMAGUCHI, T., NARUSHIMA, Y., OKAMURA, S., SAKAKIBARA, S., SUZUKI, C., WATANABE, K.Y., YAMADA, H. & YAMAZAKI, K. 2005 Three-dimensional anisotropic pressure equilibria that model balanced tangential neutral beam injection effects. *Plasma Phys. Control. Fusion* **47** (3), 561–567.

DENDY, R.O., HASTIE, R.J., MCCLEMENTS, K.G. & MARTIN, T.J. 1995 A model for ideal $m = 1$ internal kink stabilization by minority ion cyclotron resonant heating. *Phys. Plasmas* **2** (5), 1623–1636.

GRAD, H. 1966 Velocity gradient instability. *Phys. Fluids* **9** (3), 498–513.

GUPTA, S., CALLEN, J.D. & HEGNA, C.C. 2002 Violating Suydam criterion produces feeble instabilities. *Phys. Plasmas* **9** (8), 3395–3401.

HIRSHMAN, S.P. & BETANCOURT, O. 1991 Preconditioned descent algorithm for rapid calculations of magnetohydrodynamic equilibria. *J. Comput. Phys*. **96** (1), 99–109.

ITER PHYSICS BASIS EDITORS, ITER PHYSICS EXPERT GROUP CHAIRS AND CO-CHAIRS, ITER JOINT CENTRAL TEAM AND PHYSICS INTEGRATION UNIT 1999 Chapter 1: Overview and summary. *Nuclear Fusion* **39** (12), 2137–2174.

JOHNSON, J.L., KULSRUD, R.M. & WEIMER, K.E. 1969 Application of the energy principle to Astron-type and other axisymmetric devices. *Plasma Phys*. **11** (6), 463–472.

KRUSKAL, M.D. & OBERMAN, C.R. 1958 On the stability of plasma in static equilibrium. *Phys. Fluids* **1** (4), 275–280.

MOTOJIMA, O., OHYABU, N., KOMORI, A., KANEKO, O., YAMADA, H., KAWAHATA, K., NAKAMURA, Y., IDA, K., AKIYAMA, T., ASHIKAWA, N., *et al.* 2003 Recent advances in the LHD experiment. *Nucl. Fusion* **43** (12), 1674–1683.

NÜHRENBERG(NÉE SCHWAB), C. 1993 Ideal magnetohydrodynamics: global mode analysis of three-dimensional plasma configurations. *Phys. Fluids* B **5** (9), 3195–3206.

ROMBA, T., SUZUKI, Y. & PROLL, J.H.E. 2021 Analysis of influences of pressure anisotropies on the 3D MHD equilibrium in LHD. *Phys. Plasmas* **28** (4), 042504.

SUGAMA, H. & WAKATANI, M. 1989 Relation between growth rate of the suydam mode and that of low mode number interchange instability. *J. Phys. Soc. Japan* **58** (4), 1128–1130.

WATANABE, K.Y., SAKAKIBARA, S., NARUSHIMA, Y., FUNABA, H., NARIHARA, K., TANAKA, K., YAMAGUCHI, T., TOI, K., OHDACHI, S., KANEKO, O., *et al.* 2005 Effects of global MHD instability on operational high beta-regime in LHD. *Nucl. Fusion* **45** (11), 1247–1254.

YAMAGUCHI, T., WATANABE, K.Y., SAKAKIBARA, S., NARUSHIMA, Y., NARIHARA, K., TOKUZAWA, T., TANAKA, K., YAMADA, I., OSAKABE, M., YAMADA, H., *et al.* 2005 Measurement of anisotropic pressure using magnetic measurements in LHD. *Nucl. Fusion* **45** (11), L33–L36.